Meteoritics & Planetary Science 37, 1095–1105 (2002)
Available online at http://www.uark.edu/meteor

Ponded deposits on asteroid 433 Eros

A. F. CHENG[1]*, N. IZENBERG[1], C. R. CHAPMAN[2] AND M. T. ZUBER[3]

[1]Applied Physics Laboratory, The Johns Hopkins University, 11100 Johns Hopkins Road, Laurel, Maryland 20723, USA
[2]Southwest Research Institute, 1050 Walnut Street, Suite 426, Boulder, Colorado 80302, USA
[3]Department of Earth, Atmospheric, and Planetary Sciences, Massachusetts Institute of Technology, Cambridge, Massachusetts 02139, USA
*Correspondence author's e-mail address: andrew.cheng@jhuapl.edu

(Received 2001 November 19; accepted in revised form 2002 May 8)

Abstract–In late January 2001 *the NEAR–Shoemaker* spacecraft performed low-altitude passes over the surface of 433 Eros. Coordinated observations of the asteroid surface were obtained at submeter resolution by the NEAR laser rangefinder and the multispectral imager. This paper presents three independent, coordinated observations of a 90 m pond adjacent to a granular debris flow, including the highest resolution altimetric measurements of ponded deposits on Eros. The ponded deposits appear to have been emplaced by fluid-like motion of dry asteroidal regolith. A simple model of seismic agitation from impacts is developed to account for pond formation on Eros. The model predicts that ponds should form readily on Eros but not on the Moon, where ponds are not observed. The model also suggests that the absence of observable ponds in the largest craters of Eros, as well as on Phobos and Deimos, may be related to regolith depth.

INTRODUCTION

The near-Earth asteroid rendezvous (NEAR) mission (Cheng *et al.*, 1997) has measured the shape and surface morphology of asteroid 433 Eros from orbit using the pulsed solid-state laser altimeter NEAR laser rangefinder (NLR) (Zuber *et al.*, 2000; Cheng *et al.*, 2002) and the charge-coupled device camera multispectral imager (MSI) (Veverka *et al.*, 2000). Detailed descriptions of these instruments were given by Cole *et al.* (1997) and Hawkins *et al.* (1997), respectively. During a low-altitude flyover on 2000 October 26, which yielded observations at a minimum range of 6.4 km, NEAR found evidence of puzzling regolith processes (Veverka *et al.*, 2001a), including the first images of smooth, flat deposits in the bottoms of craters which were referred to as "ponds". Simultaneous altimetry of one of these surprising ponded deposits found a surface that was level to within 2 m over a 60 m span (Cheng *et al.*, 2001), so it was close to a constant gravitational-centrifugal potential.

The landing of *NEAR–Shoemaker* on Eros fortuitously occurred within a pond (Veverka *et al.*, 2001b). The final descent images showed a transition from a blocky surface to an smooth morphology in the pond. Additional analyses of image data clarified the nature of ponds on Eros (Robinson *et al.*, 2001). Ponds are characterized by smooth, level surfaces that are sharply delineated; they are found preferentially at low latitudes and in the bottoms of craters, although not in craters >1 km diameter; they have slightly bluer color than surrounding terrain. The level pond surfaces suggested an emplacement mechanism involving fluid-like motion with minimal resistance to shear, although small, steep-walled features are observed within them, such as the collapse feature noted by Veverka *et al.* (2001b) within the pond where *NEAR–Shoemaker* landed and other examples noted by Robinson *et al.* (2001). These steep-walled features show that these pond deposits are not presently fluid-like, but cohesive. The smooth surfaces of ponds indicate a size-sorting mechanism (Robinson *et al.*, 2001), although the image resolution should be kept in mind. The best image resolution obtained in a pond was 2 cm during the NEAR landing. For ponds imaged from 35 km orbit, the image resolution was ~4 m. Robinson *et al.* (2001) suggested that electrostatic levitation of fines may play a role in formation of ponds on Eros.

The topography of the ponds is key to understanding their nature. Of special interest is the degree to which the surface of a pond conforms to an equipotential, meaning the combined gravitational and centrifugal potential calculated from a shape model for Eros determined from NLR data (Zuber *et al.*, 2000):

$$\Phi(\mathbf{x}) = -\int d^3\mathbf{x}' \frac{G\rho}{|\mathbf{x}-\mathbf{x}'|} - \frac{\Omega^2 r^2}{2}$$

integrated over the volume of the asteroid, where r is the distance from the point $\mathbf{x}$ to the rotation axis, and Ω is the rotation rate 3.31166×10^{-4} rad s^{-1}. The geopotential height h measured in meters is defined by

Prelude preprint MS#4699

$$h(\mathbf{x}_i) = \left|\Phi(\mathbf{x}_i)/g_{\text{avg}}\right|$$

where g_{avg} is the local average magnitude of the effective gravitational acceleration. For the pond observed on 2000 October 26, g_{avg} was 0.43 cm s^{-2}, which is much less than on planetary-sized objects. This value of surface gravity is an intermediate value for Eros, where the total variation of the surface gravity across the surface is about a factor of 2 (Veverka *et al.*, 2000; Zuber *et al.*, 2000). Since the level surface is the key evidence for fluid-like emplacement (Veverka *et al.*, 2001b), it is important to investigate the topography of additional ponds.

The next section presents high spatial resolution NLR and MSI observations of a second pond and an adjacent debris flow on Eros. The term "debris flow" will be used to mean downslope motion of material with a degree of coherence, without any implication of speed or triggering mechanism, and without implying presence or absence of fluid. This pond and debris flow were observed on three independent occasions, 2000 December 21 as well as 2001 January 26 and 28, allowing an accurate determination of the elevation *change* across the pond. These are the highest resolution topographic measurements of any pond on Eros. The following section develops a model for mass motion induced by seismic shaking from impacts on Eros, which would cause redistribution of unconsolidated surface materials and contribute to pond formation. This model is proposed as an alternative to electrostatic levitation as a mechanism for mobilization of regolith. The conclusion compares some predictions of seismic shaking and electrostatic levitation with observations from Eros, the Moon, and the satellites of Mars.

OBSERVATIONS OF 2001 JANUARY 26 AND 28

The low-altitude flybys of 2001 January 26 and 28, yielded data from minimum ranges of 4.8 and 3.1 km, respectively, including the highest resolution, coordinated NLR and MSI observations of ponds from the entire orbital mission. While higher resolution images were obtained during the final descent to the surface on 2001 February 12, the spacecraft ephemeris from the final descent has not been determined with sufficient accuracy to permit determinations of topography. The coordinated NLR and MSI data consist of overlapping images obtained during an NLR track, meaning a series of NLR measurements. The NLR boresight direction, which is illuminated by the laser, is fixed close to the center of the MSI image field-of-view (Cheng *et al.*, 2000, 2001). As the surface moves past the NLR boresight owing to orbital motion, asteroid rotation, and spacecraft maneuvers, the laser spots trace out a track along which ranges are measured and surface elevations are determined. For the 2001 January 28 observations of the pond, successive laser spots were separated by an average of 5.2 m center-to-center, and the spot diameter was 0.87 m, so the NLR track was under-sampled. NLR was designed to operate in a 50 km orbit from which it measures a contiguous track. On 2001 January 26 the spot spacing and diameter were 4.9 and 1.25 m, respectively. NLR's range precision is ~1 m at 40 km range and ~0.5 m under 20 km range (Cheng *et al.*, 2000).

The highest resolution topographic measurements of ponds from *NEAR–Shoemaker* were obtained from the low-altitude flyovers of 2001 January 26 and 28. One 90 m diameter pond, located near an end of the asteroid at 2.55° S, 179° W, was observed by both MSI and NLR on both dates. This pond and its surrounding region are shown in a context image (Fig. 1) obtained from 35 km orbit on 2000 December 21. Figure 1 shows a second pond that was not sampled by NLR—since the NLR boresight is fixed close to the center of the image frame, NLR does not sample the majority of ponds found in images.

Figure 1 shows that the pond of interest is located in a 180 m crater that is itself within the wall of a ~800 m wide, severely degraded crater which is nonetheless clearly visible in the altimetric tracks of Fig. 2. Figure 2 shows geopotential height (or "elevation") *vs.* distance for the NLR track from 2000

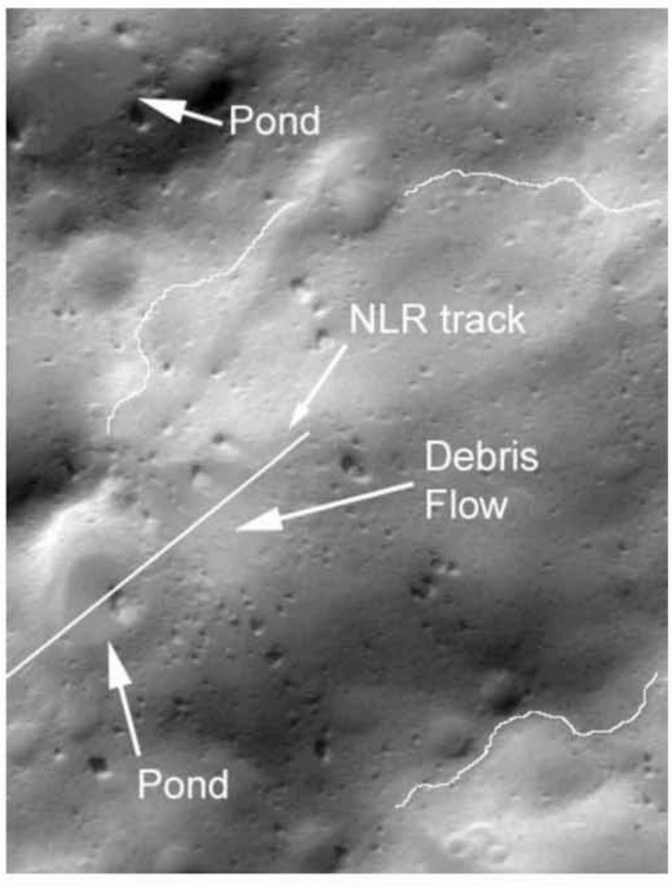

FIG. 1. Debris flow and pond 2.55° S, 179° W; image M0152775525 obtained 2000 December 21 at 16.6 km range in the 950 nm filter. The NLR track of Fig. 2, indicated by a white line, crosses a pond and debris flow within the wall of an 800 m degraded crater sketched by the thin white curve. A second pond is found at upper left. Illumination is from the bottom right.

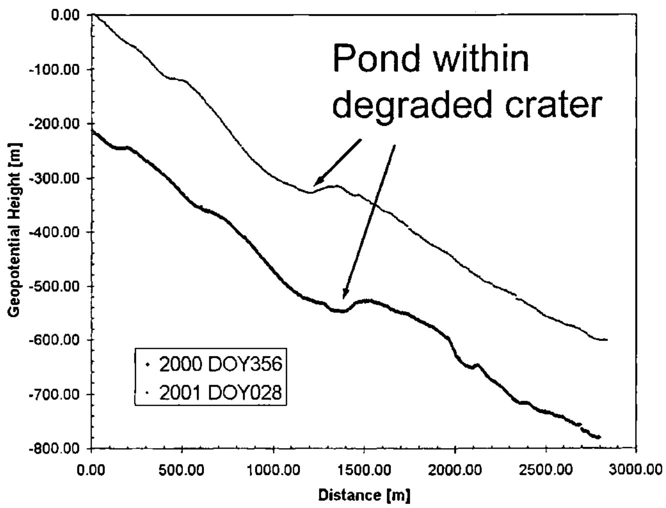

FIG. 2. Two NLR tracks through the same site, pond and nearby debris flow on the wall of a degraded crater, obtained 2001 January 28 (upper curve) and 2000 December 21 (DOY 356). Geopotential height and distance have arbitrary reference values.

December 21 that was obtained simultaneously with the image in Fig. 1, together with the altimetry from 2001 January 28 plotted on the same scale. Distance is defined using the line that is the least-squares best-fit to a short track of laser spots in three dimensions. The position of each laser spot is projected onto this line, and distance is measured along the line. Elevation and distance have arbitrary reference values. The procedure is equivalent to reading off distances from a straight-edge. For short tracks, spacecraft ephemeris uncertainties are slowly varying and result in absolute position uncertainties, both in horizontal and vertical directions, whereas elevation *differences* are determined to within the instrument precision. Figure 2 shows the degraded 800 m crater to be located within a regional slope, with the pond found at a local minimum of elevation, although it is well offset from the center of the confining crater. Neither the 800 m crater nor the 180 m crater containing the pond has a raised rim.

The average slope along either of the tracks in Fig. 2 is ~12°, a typical value for the surface of Eros (Zuber *et al.*, 2000). In this case, as was true for the pond observed in the October 26 low-altitude flyby (Cheng *et al.*, 2001), the regional slopes are well below expected angles of repose for particulate material, 30° to 40° depending on particle sizes, shapes and material properties. Hence, downslope movement from slope failures in this region would not be expected in the absence of a triggering mechanism such as seismic shaking from impacts (Houston *et al.*, 1973; Schultz and Gault, 1975).

The locations of three NLR tracks relative to the pond are shown in Fig. 3, where the tracks are plotted on an image mosaic obtained 2001 January 28 at a resolution of 36 cm per pixel. The NLR boresight relative to the MSI field-of-view was determined for the full set of 2001 January 28 observations to be at line number 220 ± 2, sample number 260 ± 2 using the methods of Cheng *et al.* (2001). Line and sample numbers are defined in the rectified MSI pixel format of 412 lines and 537 samples, where each pixel is square and subtends 95.9 μrad. Comparison with Fig. 1 (the lines run the larger dimension of the frame) shows that the NLR tracks were off-center relative to the 800 m degraded crater and did not measure its full depth.

Figure 3 shows not only the two NLR tracks of Fig. 2, but also a third track across the pond obtained on 2001 January 26. In Fig. 3, roughly within the region between the markings "31" through "41", are found morphological features interpreted as indicating a debris flow. These features include a smooth, undulating surface with lower boulder density than surrounding terrain; embayment of the confining boundary; and presence of upslope ramparts at obstructions to the suggested flow. The margins of the debris flow (to the left in Fig. 3) are lobate in plan. These margins appear to reflect embayment of confining topography, namely, the relatively steep wall of the 800 m degraded crater. The pond at the upper left in Fig. 1, which was not sampled by NLR, also has a lobate margin. Several large (10 to 20 m) boulders within the flow region display raised slopes on their upslope sides, which may suggest residual cohesion or internal friction in a granular flow. These morphological features are consistent with occurrence of mass motion, but no obvious source region for the debris flow can be identified toward the right side in Fig. 3 or in the context image (Fig. 1); there is no scarp or evidence for any localized slope failure. Instead, the images suggest that fine particulate matter in the debris flow is mobilized relative to larger boulders. The illumination in Fig. 3 is extremely oblique, ~80° incidence relative to the pond, from the shadow length of the large boulder in the pond (height 7 m; Fig. 4). The regional downslope direction, indicated in Fig. 3, is the projection of the surface effective gravity vector first into the local average surface (using a shape model for Eros) and then into the image plane.

A beach-like morphology is noted around the periphery of the pond, from the lighter shading next to the pond compared to that farther away in Fig. 3. The morphology in question refers to an annular zone outside the pond, where the surface is convex upward as observed on transects oriented radially away from the center of the pond. The shading changes in this zone are consistent with slope changes similar to those found on a berm.

Figure 4 shows three independent topographic profiles of the debris flow and pond obtained on separate orbits, with the profiles offset in elevation and aligned such that the pond is centered near distance 1200 m. Figure 3 shows that two of the tracks, those obtained on 2000 DOY356 and 2001 DOY026, intersected near the pond. At this crossover point, distance 1110 m in Fig. 4, these tracks measured the same physical point, so they must have the same elevation and were so adjusted. The distance reference was established relative to a 10 m boulder sampled by the DOY026 track near the edge of the pond, which is seen at distance 1240 m in Fig. 4 and which is called out in Fig. 3. Within the 180 m crater confining the

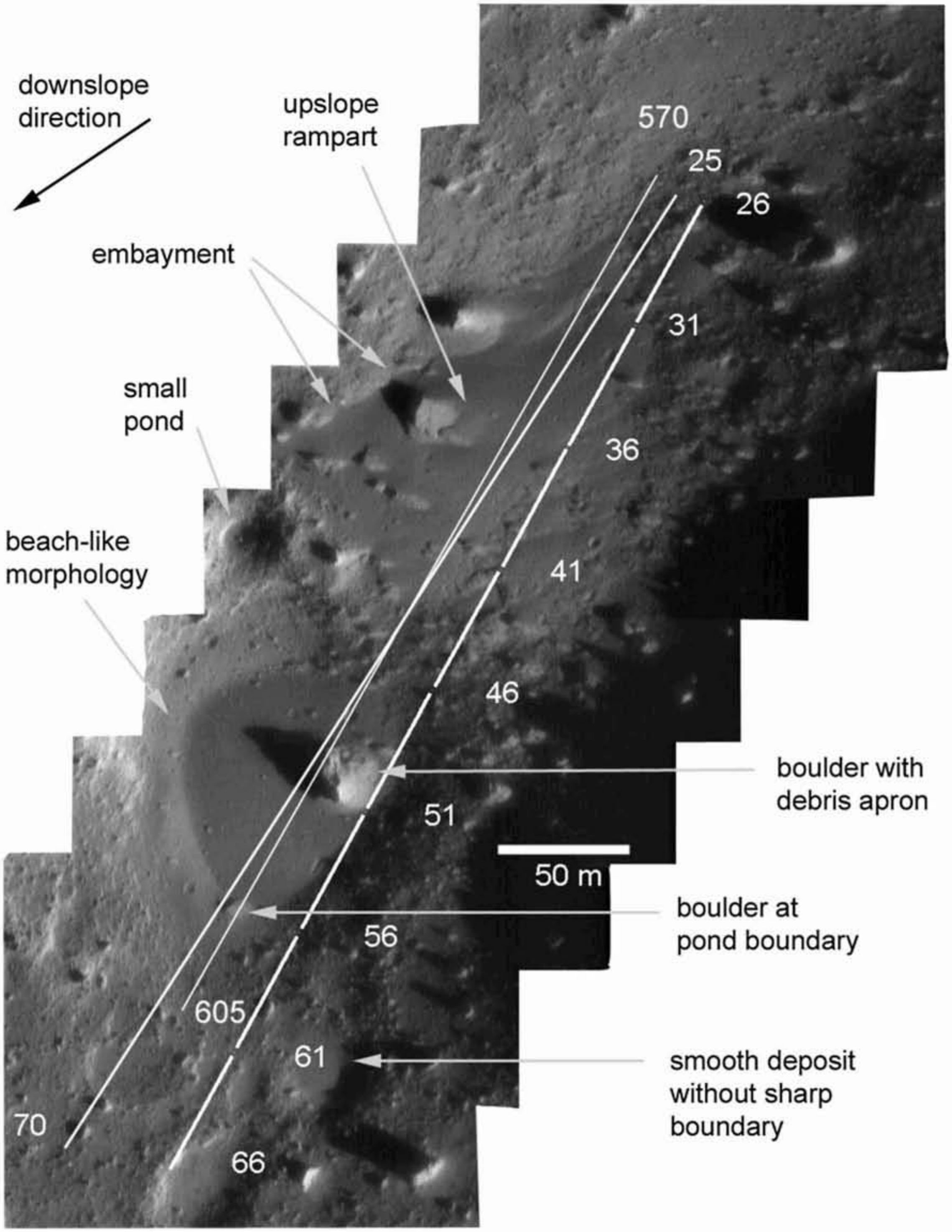

FIG. 3. MSI mosaic at 36 cm per pixel. The 2001 DOY028 track (dashed line on the right) has gaps that show the times of successive MSI frames, with the last two digits of mission elapsed time (MET) indicated. The full METs of these frames are 1560878xx. The METs of the 2000 DOY356 track (longer solid line on the left) are 1527755yy with the last two digits marked at each end. The thin solid line with three-digit numbers is the track of 2001 DOY026, at the METs 155888zzz. The black arrow is the regional downslope direction based on a shape model with 400 m resolution. Illumination is from the lower right side of the mosaic.

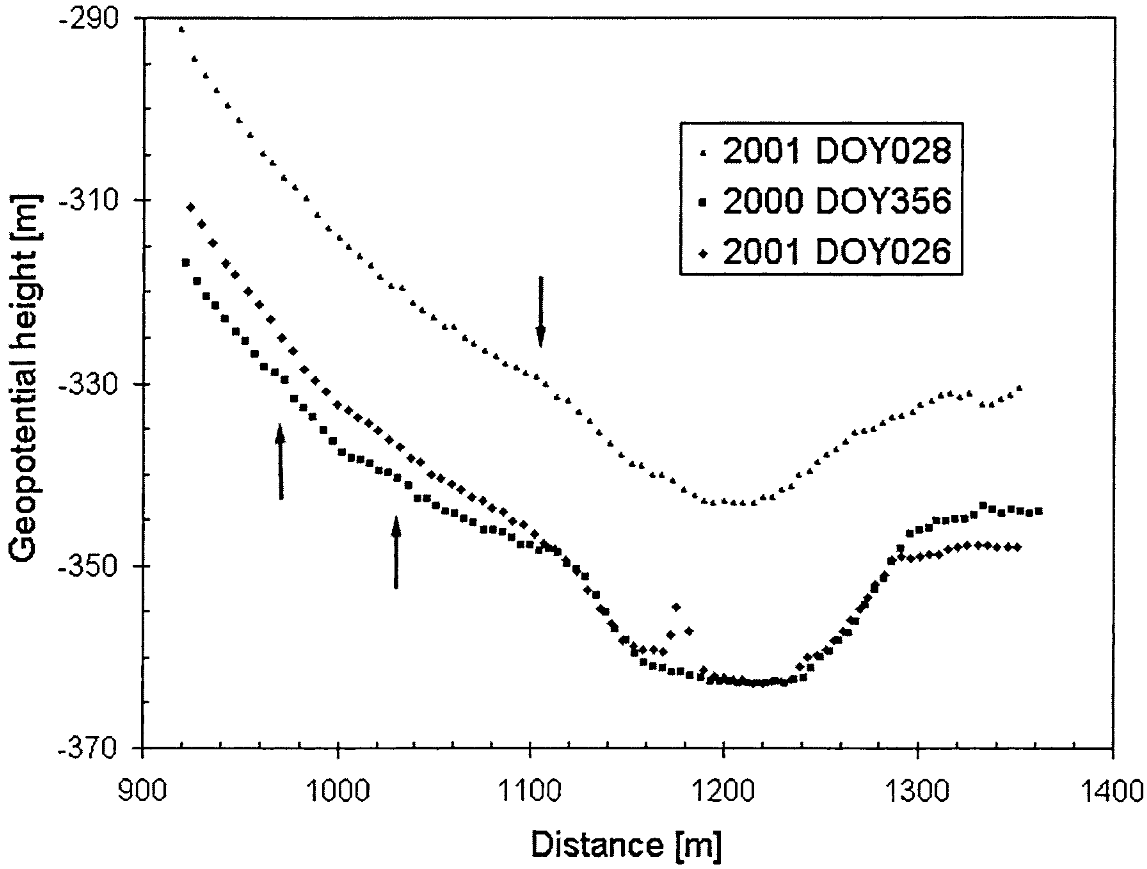

FIG. 4. Elevation profiles of debris flow and pond (with arbitrary height offset to DOY028 track). The January 26 profile (diamonds) sampled a 7 m high boulder within the pond around distance 1180 m and a boulder 10 m wide around distance 1240 m. Small arrows mark features in the debris flow suggestive of shallow deposits.

pond, these two adjusted tracks in Fig. 4 agree to ~0.5 m, which is the instrumental precision, except for two boulders sampled by the DOY026 track. These are the 10 m wide boulder just mentioned and the large boulder within the pond, which was at distance 1180 m and which can be seen in Fig. 3 to have a prominent debris apron.

The DOY356 track and the DOY026 track are both central and show that the pond elevation is ~1.6 m higher on the side toward the debris flow in Fig. 3, compared to the opposite side 82 m away. Both NLR tracks also show evidence of curvature in the surface of the pond. Moreover, these NLR tracks show distinct slope changes circa distances ~1150 and ~1240 m, consistent with the limits of the level pond surface in Fig. 3. These data are consistent with indications from images that a break in slope defines pond margins. Finally, the 2001 DOY028 track, closer to the edge of the pond, also shows a higher elevation on the side toward the debris flow. The topographic profiles show that the pond surface, while close to level, does deviate measurably from an equipotential. Shading changes in the images of the pond surface (Fig. 1) also support the existence of curvature.

The debris flow is located on a slope at an elevation averaging ~20 m above that of the pond. The region between the debris flow and the pond is the bouldery rim of the 180 m crater enclosing the pond (near the marking "46" in Fig. 3, and distance 1110 m in Fig. 4). Figure 4 shows an elevation drop of ~12 m from the crater edge to the pond surface. This elevation change and the downward slope of the pond away from the debris flow suggest that the debris flow may have been a source of ponded fines. The profiles in Fig. 4 also show topographic features that suggest a shallow depth of a few meters in the debris flow. The slope changes may reflect underlying topography or occurrence of multiple flow episodes. The depth of the pond is estimated from the 180 m diameter of the confining crater; prior to the ponded deposit, the crater depth would have been ~20 m assuming an average depth-to-diameter ratio of 0.11 (Barnouin-Jha *et al.*, 2001), so from Fig. 4 the pond is at most ~6 m deep, consistent with depth estimates from images (Robinson *et al.*, 2001).

In Fig. 3, a pond is adjacent to, lower than, and sloping away from a debris flow which may be a source of fines, suggesting that fluid-like movement is associated with pond formation. However, isolated ponds can be found without a nearby debris flow on Eros, and an example is seen in Fig. 1. The present pond may be adjacent to a debris flow by chance.

SEISMIC SHAKING AND POND FORMATION

Ponds on Eros display level, sharply bounded surfaces. Robinson *et al.* (2001) found that large ponds >30 m have a non-uniform distribution over the surface of Eros that is concentrated to low latitude, similar to the distribution of places that spend the most time near the terminator. Pond formation evidently involves settling of fines in gravitational lows. For the pond of Fig. 3, "fines" must be <<40 cm; for the pond in which *NEAR–Shoemaker* landed, "fines" must be much less than centimeter size. Robinson *et al.* (2001) suggested that electrostatic levitation of fines may play a role in pond formation on Eros. From previous work, particles on the order of 100 μm may be electrostatically levitated on Eros (*e.g.*, Lee, 1996). Several other mechanisms have been suggested for mobilization of regolith on Eros, including seismic shaking following impacts which can also produce size-sorting (Veverka *et al.*, 2001a; Asphaug *et al.*, 2001). This section will present a model for pond formation from seismic shaking and will apply this model not only to Eros but also to the Moon, where ponds are not observed. In this model, regolith is mobilized by seismic agitation, and the pond boundary is what appears between an almost level pond surface and a bowl-shaped confining volume, when the bowl is partially filled with fines emplaced in a fluid-like manner. Regolith mobilization from seismic shaking may have important implications for degradation of surface topography on asteroids, but the present discussion will focus on ponds.

A full discussion of electrostatic levitation would be beyond the scope of this paper. The key issues are the particle size fraction that can be levitated on an asteroid and the heights of levitation. If dust is to be levitated and still affected by gravity so as to fall back downhill from where it originated, as suggested by Lee (1996), there must be a balance between the weight of the grain and the electrostatic force, such that the grain is lifted only a small distance relative to the local topography. Such a balance may apply to only a particular size fraction of the dust population, whereas for most grains either the gravity dominates (levitation fails) or the electrostatic force dominates (grains are lifted too high or escape from the asteroid). Only the fraction of grains lofted to low enough altitude would fall back to the surface locally downslope from where they were levitated. If grains falling back to the asteroid were most likely levitated by electrostatic forces well above local topography, the result would be a relatively uniform mantling of the surface rather than filling of ponds in gravitational lows. However, the balance between electrostatic force and gravity is uncertain and depends on poorly known properties such as particle shapes, electrical resistivity and photoelectron yields. This paper considers an alternative mechanism, seismic shaking, for mobilization of regolith.

A dry granular material can exist stably in a slope below the angle of repose, but can then be mobilized by agitation to modify slopes (Houston *et al.*, 1973; Schultz and Gault, 1975) or create a debris flow (Iverson, 1997). Figure 5 sketches how fluid-like movement of fines mobilized by seismic agitation can create ponded deposits. The hypothesized process invokes a continued interaction of boulders with a consolidated substrate during shaking, to induce a relative motion between the fines and the boulders (meaning a size large enough to rest upon the consolidated substrate and to protrude above the shallow layer of unconsolidated fines), because the boulders can move downslope only to a limited extent compared with fines. This

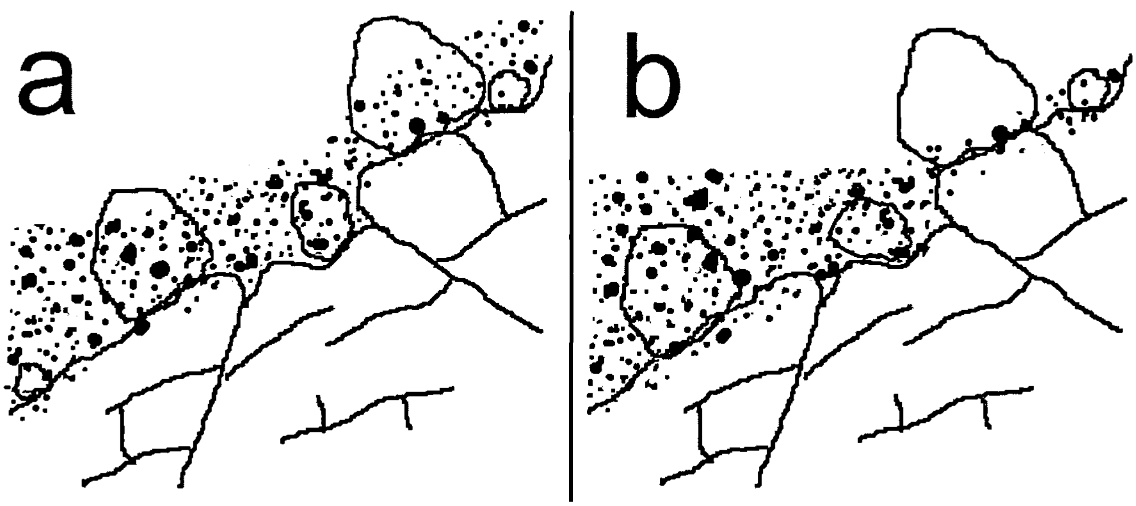

FIG. 5. Sketch of hypothesized process, before seismic agitation (a) and after (b). A shallow layer of fines (dots of various sizes) and boulders rests upon a fractured, consolidated substrate. Fines can support shear stresses unless actively shaken. During shaking, fines are mobilized like a fluid, but boulders are impeded by underlying topography. After shaking, the free surface of the pond is level, and some boulders are covered.

picture invokes gentle shaking that causes slope failure without tossing boulders many meters. The boulders may not rest directly on the consolidated substrate but may be coupled to it mechanically *via* a thin, compressible layer of fines, which would attenuate the transmission of seismic accelerations to the boulders. The model predicts a terrain where topographic highs (*e.g.*, crater rims or ridges) appear more bouldery whereas topographic lows appear smoother because they become filled with fine particulates and many boulders are covered. Indeed, for the NLR data obtained during the 2000 October 26 observations of a different pond, a fractal roughness analysis showed that topographic highs (in this case, ridges) were rougher than lows (Cheng *et al.*, 2001). Finally, in some cases alignments are observed of boulders and positive relief features on Eros, suggestive of these boulders resting upon linear structural features in a buried, consolidated substrate (Cheng *et al.*, 2001; Veverka *et al.*, 2001a,b).

Merely leaving behind or burying the large (several meter) boulders, as suggested in Fig. 5, may not explain completely the degree of size-sorting observed in ponds. While the present observations constrain the pond surface to be smooth at resolutions <1 m, images obtained during the final descent to the surface show a pond surface to be smooth at centimeter-resolution (Veverka *et al.*, 2001b). If this pond is typical, then pond formation sorts out particles smaller than a centimeter. However, various size-sorting mechanisms can operate in granular media under repeated shaking (Asphaug *et al.*, 2001) driven by circulation of fines and/or wedging of fines into dilated spaces over or under larger objects ("kinetic sieving", see below). Most geological experience with terrestrial debris flows does not apply to Eros because of the absence of liquid water. Terrestrial debris flows typically concentrate large sediment clasts and entrained objects at their surge heads, owing largely to the action of water in the flows (Iverson, 1997). Instead, relevant information on size-sorting in dry granular flows can be gleaned from laboratory experiments and numerical simulations (Jaeger *et al.*, 1996).

When dry, granular media are shaken in the laboratory or agitated and/or poured out of containers, tubes, or chutes, size sorting is typically observed (*e.g.*, Rosato *et al.*, 1987). One important mechanism is circulation of fines driven by frictional interaction with the walls of the container. In laboratory experiments, the magnitude and even the sign of the circulation depend on the shape of the container (Knight *et al.*, 1993). This circulation can lift large objects and leave them stranded on the surface, or, instead, bury them as would be required to explain ponds on Eros. Burial of large objects occurs in outward slanted containers with boundary slip (*i.e.*, a conical "crater"). Such interactions are critically affected by the boundary surface and whether it imposes a no-slip or limited-slip condition on adjacent grains whose size is of the order of the wall roughness (the velocity profile of much finer grains is not affected by wall roughness; for example, Savage, 1979, 1984). On Eros, roughness has been determined only down to scales of a few meters, where fractal behavior is observed (Cheng *et al.*, 2001, 2002).

Size-sorting in granular media undergoing shaking can also be driven by kinetic sieving (*e.g.*, Rosato *et al.*, 1987; Shinbrot and Muzzio, 1998). Large particles can be brought to the surface by falling of fines through gaps between them. Large particles can also be wedged upwards during agitation as fines avalanche into temporary voids beneath them. Kinetic sieving has been proposed as a mechanism to bring boulders to the surface at Eros, although it can also operate to bury them (Asphaug *et al.*, 2001).

In summary, the occurrence of size sorting in granular flows is well established by laboratory experiments, but it is not clear if such sorting suffices to explain the apparent concentration of fines into at least some ponds on Eros.

Seismic Shaking Model

In Fig. 3, the surfaces of the pond and debris flow display impact craters up to 6 m diameter, allowing estimation of a crater age. For a rough estimate, the lunar impact flux is adopted, neglecting two complications with opposing consequences—lack of gravitational focusing reduces the impact flux on Eros, but its orbit brings Eros closer to the asteroid belt and increases the flux. The orbit of Eros evolves chaotically (Michel *et al.*, 1998), and it is not possible to reconstruct when Eros left the Main Belt or where it formed. The assumed impact flux (Melosh, 1989) is approximated by

$$\begin{cases} F = 5.6\times10^{-23}L^{-3.48} \quad \mathrm{m^{-2}\ s^{-1}}, \quad 10^{-4} < L < 3.2\ \mathrm{m} \\ F = 1\times10^{-23}L^{-2} \quad \mathrm{m^{-2}\ s^{-1}}, \quad L > 3.2\ \mathrm{m} \end{cases} \tag{1}$$

where L is impactor diameter in meters. Here F is the cumulative flux of impactors larger than L.

Conventional impact scaling relations (Holsapple, 1993) are adopted

$$\begin{gathered} \pi_V = K\left[\pi_2\left(\frac{\delta}{\rho}\right)^{1/3} + \pi_3{}^{(2+\mu)/2}\right]^{-3\mu/(2+\mu)}, \\ \pi_2 = \frac{ga}{u^2}, \qquad \pi_3 = \frac{Y}{\rho u^2} \end{gathered} \tag{2}$$

this form interpolates between the strength and gravity regimes, where π_V is the ratio of crater to impactor volume, g is surface gravity (near the ends on Eros, typically 0.003 m s^{-2}), a is projectile diameter, u is impact speed, Y is effective strength in the target, and δ and ρ are the impactor and target densities (here 2.7 and 1.4 g/cc, respectively). In what follows the values $K = 0.24$, $\mu = 0.41$, and $Y = 0.018$ MPa are adopted, as appropriate for a dry soil with a strength typical of lunar soils

(Holsapple, 1993; Houston *et al.*, 1973). For an impact speed of 8 km/s under these conditions, the transition between strength and gravity scaling occurs around a crater size of 300 m.

These relations predict that a 6 m crater is made by a 20 cm projectile impacting at 8 km s^{-1}, in the strength regime. For a cumulative impact flux of projectiles above 20 cm equal to 1.5×10^{-20} m^{-2} s^{-1}, and for a target area (pond and debris flow) of 15 000 m^2, the age would be $\sim 10^8$ years since the last time the surface was mobilized and fluid-like to an extent that small craters would be effaced. This estimate is extremely uncertain, because of the uncertain orbital history (Michel *et al.*, 1998), and because the effective strength on Eros may increase significantly with depth, which would require a larger projectile to make the same-sized crater.

The rate at which impacts should mobilize unconsolidated, fine particulates by seismic agitation can also be estimated. Slope failures can be triggered by agitation when seismic accelerations become comparable to the effective acceleration of gravity (Houston *et al.*, 1973). The accelerations that would result from impacts can be estimated using seismic data from large terrestrial explosions, which can be fitted by the empirical relation (Carder and Cloud, 1959; Adushkin and Nemchinov, 1994):

$$a = 9.4\ (E/10^{11}\ \mathrm{J})^{0.75}\ D^{-2}\ \ \mathrm{cm\ s^{-2}} \qquad (3)$$

where a is the acceleration, E is $0.1\times$ the impact energy (Melosh, 1989), and D is the distance in kilometers from the impact. This relation applies in the near field where seismic waves propagate spherically and energy absorption can be neglected (typically 200 km on Earth). At large distance D, seismic energy is typically damped (Carder and Cloud, 1959) by a factor $\exp(-0.002D)$, but the damping varies greatly with rock and soil type. Eros has a mean diameter of only 17 km, so seismic energy from an impact causes ringing in the body with an exponential decay time estimated by 160 s for a typical seismic wave speed of 3 km/s. After an impact, the initial value of global average seismic acceleration is estimated by Eq. (3) with $D = 17$ km, and the acceleration decays thereafter with a 160 s time constant. For example, an 8.5 m projectile impacting at 8 km s^{-1} will initiate a global average acceleration of 0.4 cm s^{-2} and will mobilize fine particulates for ~200 s. For expected seismic frequencies of a few hertz (Carder and Cloud, 1959), the corresponding amplitudes are approximately millimeter.

To create a level pond deposit in this picture, seismic acceleration comparable to the local gravity must be sustained for a sufficient time that fluid-like motion can equilibrate, namely, several times the propagation time of shallow gravity waves across the pond. The propagation speed of these waves (Landau and Lifshitz, 1959) is estimated as $\sqrt{gh}$ where g is the effective gravity and h is the depth of the pond. The propagation time is 600 s for an 80 m pond of 6 m depth, with the local gravity 0.3 cm s^{-2}. Hence the pond observed on 2001 January 28 is too large to equilibrate after a single impact, but tens of impacts are required. Indeed, at present the pond still retains a measurable elevation difference from one side to the other.

Alternatively, the propagation time of a gravity wave as used above may not be appropriate if there is significant friction as in a cohesive lunar-like regolith, in which case the damping time of the seismic excitation may be the appropriate time scale. The latter damping time in lunar regolith is tens of minutes (Wilhelms, 1984), which is comparable to the propagation time for the present pond. A seismic damping time longer than the propagation time would enhance equilibration of the pond and reduce the present-day residual elevation difference across it. A seismic damping time close to, or less than, the propagation time would not affect the conclusion of the previous paragraph.

The finding of a berm-like structure in the annular zone around the periphery of the pond (Fig. 3) is consistent with action of shallow gravity waves in the pond. Excitation of such waves by seismic shaking may result in deposition of fines from the pond to form a sediment platform.

An impact destroys nearby ponds, even as its seismic shaking contributes to forming ponds farther away. Seismic jolting (Greenberg *et al.*, 1996) at amplitudes sufficient to disrupt the surface, and secondary impacts, contribute to destruction of ponds. Covering by crater ejecta is also important on the Moon, but is evidently not important on Eros where localized ejecta blankets are not observed (Veverka *et al.*, 2000), although most of the blocks may have originated in an impact that made Shoemaker crater (Thomas *et al.*, 2001). For a simple model, it is assumed that ponds within two crater diameters of an impact are destroyed on Eros or the Moon, whereas seismic shaking at greater distances may contribute to pond formation as long as the acceleration Eq. (3) exceeds the surface gravity. In a more detailed model, the distance from an impact out to which ponds are destroyed, scaled in terms of crater diameter, may not be precisely equal on Eros and the Moon. In addition, ejecta distributions on Eros are affected by the irregular shape and relatively rapid rotation. The absence of contiguous ejecta blankets on Eros may allow a smaller destruction radius than two crater diameters, which would further enhance pond formation on Eros by seismic shaking. The simple model of Fig. 6 uses a destruction radius of two crater diameters for both Eros and the Moon.

Figure 6 shows that on Eros, panel (a), the surface gravity is so low that even 14 cm projectiles can produce enough seismic shaking to promote pond formation at large distances compared to the crater diameter. Impact of an 8.5 m projectile, as mentioned above, can promote pond formation all over Eros, but destroys ponds over only a small fraction of Eros's area. This contrasts with the behavior that the same simple model would predict for the Moon, assuming the same parameter values except for impact velocity which is assumed to be 14 km/s in the lunar case. In particular, the same K, μ, and Y are adopted as before. As shown in Fig. 6, the small (<10 cm) impactors on the Moon can only destroy ponds, because of the larger lunar

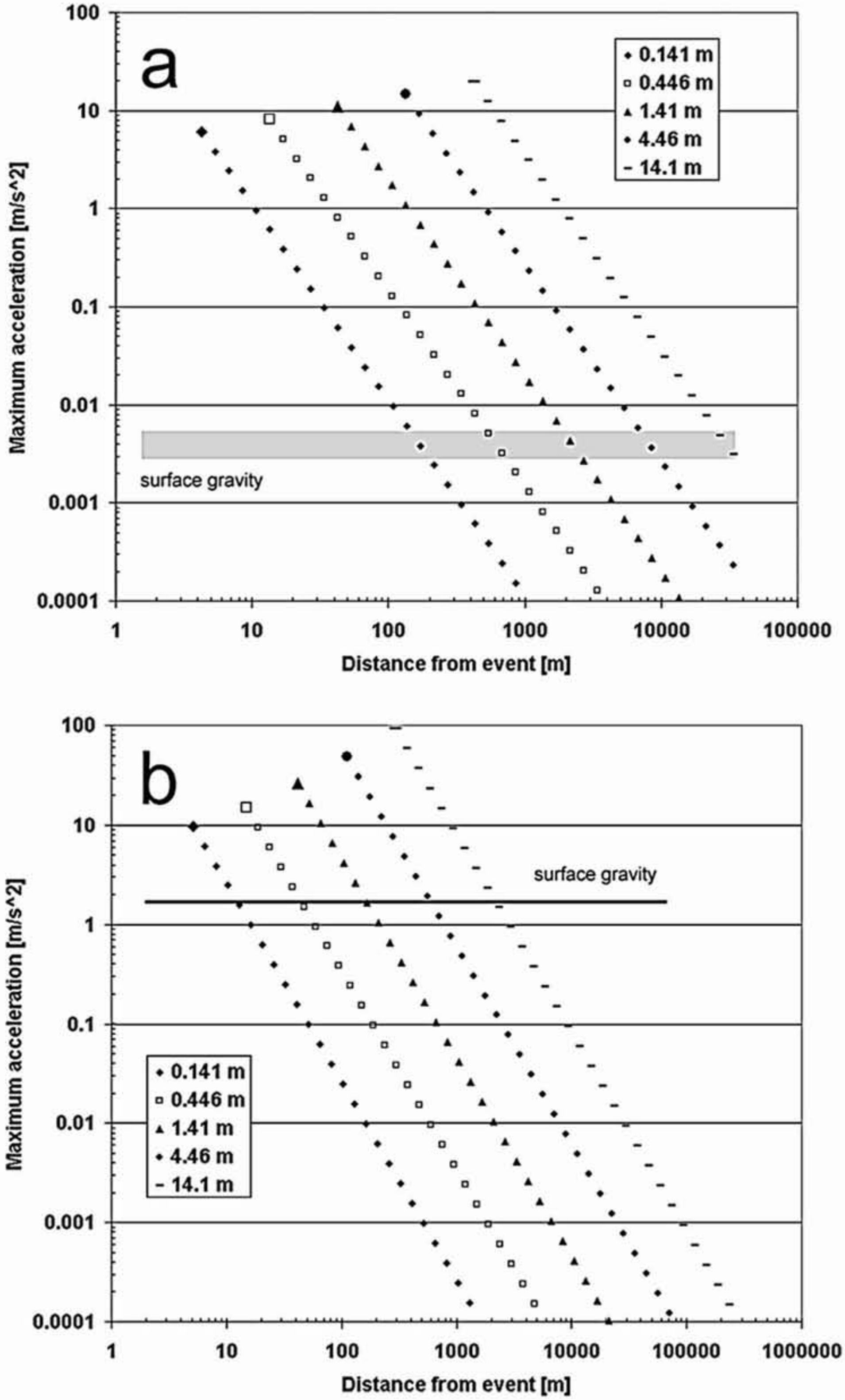

FIG. 6. Seismic shaking, maximum acceleration *vs.* distance from impact: Eros (a) and Moon (b) for five projectile diameters, at 8 km/s for Eros and 14 km/s for the Moon. The shaded bar represents the range of surface gravities on Eros. The large symbols are plotted at a distance equal to the crater diameter, and ponds are assumed to be destroyed out to twice this distance.

gravity. An impact of a 14.1 m projectile would promote ponding out to a distance of only ~2 km, not very large compared to the crater diameter ~300 m, but any nascent ponds are continually eroded or degraded by the much more frequent small impacts.

The competition between pond destruction from impacts and pond formation from impact-induced shaking can be quantified using the size distribution Eq. (1). The differential size distribution (projectiles per square meter per second in a differential size range) is multiplied by the area over which ponds are destroyed by these impacts; this quantity is then integrated numerically over projectile sizes to estimate a average pond destruction rate. For Eros, destruction occurs at a rate of 1.1×10^{-7} per year, and for the Moon, it is at 1.7×10^{-7} per year. Similarly, a pond formation rate is estimated using a pond formation area for an impact of a given size, where the formation area is estimated as πD^2 with D the distance out to which the seismic acceleration exceeds the surface gravity (provided the formation area is less than the total area of the object, which is for Eros 1100 km^2). After integration over projectile sizes, the pond formation rate becomes for Eros 2.2×10^{-5} per year which is ~200× the destruction rate, and which implies that on the average impacts on Eros are ~200× more likely to induce slope failure in a given area by shaking than they are to disrupt or cover the area. The analogous calculation for the Moon yields a pond formation rate of 9.2×10^{-10} per year which is much less than the destruction rate, implying that slope modification from seismic shaking is highly unlikely on the Moon compared with destruction by impacts.

It is emphasized that this seismic shaking model is conservative because two effects have been neglected, both of which would tend to further enhance pond formation on Eros relative to the Moon. The first is the likelihood already mentioned that the destruction radius, scaled to crater diameter, is greater on the Moon because of blanketing by ejecta. The second is the possibility (Chapman *et al.*, 2002) that the projectile size distribution in the asteroid belt may be depleted at small sizes when compared with the lunar distribution (1); such a size distribution, depleted of impactors smaller than ~1 m, would enhance pond formation relative to destruction in the present model. The model also assumes that seismic energy is transmitted about as efficiently as in Earth's crust and uppermost mantle. Lunar seismic velocities increase with depth from ~300 m/s at the surface to ~6 km/s at 20–25 km, where they increase to ~7 km/s and remain roughly constant at greater depth (Wilhelms, 1984 and references therein). Seismic velocities on Eros are not well constrained by NEAR data, although there is strong evidence for a competent but fractured interior (Veverka *et al.*, 2000; Zuber *et al.*, 2000).

DISCUSSION AND CONCLUSIONS

The seismic shaking model predicts that ponds should form readily on Eros, but with the same assumptions, it predicts that ponds should be extremely rare on the Moon. Model parameters are uncertain, but seismic shaking appears viable as a mechanism to mobilize fines so as to degrade topography or to form ponds. This mechanism does not require fines to originate from outside the confining bowl in which the pond is found, but an external origin may be possible. The absence of raised rims for the degraded 800 m crater of Fig. 1 or for the crater containing the pond may be consistent with degradation of topography as a result of seismic shaking.

The pond and debris flow of Fig. 3 have morphological and topographic features consistent with emplacement by fluid-like motion. The surfaces of these features appear young, with craters up to 6 m, but the impact of an 8.5 m projectile, which would make a 290 m crater for the present model parameters, would induce sufficient shaking to efface such small features in ponds all over Eros. An assumed lunar impact flux would give ages of $\sim 1.4 \times 10^8$ years for a 6 m crater in the pond and debris flow, but $\sim 9 \times 10^8$ years for a globally pond-forming impact anywhere on Eros. However, even as little as 10^8 years ago, Eros may not yet have evolved out of the Main Belt (Michel *et al.*, 1998). Hence these estimates should be interpreted with caution, and they show that even young-appearing features like the pond and debris flow could have formed while Eros was still in the Main Belt. The surface of Eros may show effects of a cratering hiatus after it left the Main Belt (Chapman *et al.*, 2002). The debris apron around the boulder in the pond of Fig. 3 overlies the pond surface, but may not be much younger than 10^8 years. The seismic shaking invoked in the present model to form ponds would not necessarily disrupt a fine debris layer resting on top of the pond, but would cause it to spread.

While the seismic shaking model meets the test of predicting ponds on Eros but not on the Moon, there is another observational constraint, that ponds are not observed in craters >1 km on Eros, nor are they found on Phobos and Deimos (Robinson *et al.*, 2001; Veverka *et al.*, 2001b). However, implicit in Fig. 5 is a requirement that the depth of unconsolidated fines is at most a fraction of the depth of the confining bowl, so that a sharply bounded pond surface develops as the intersection of a smooth, flat surface with the walls of the bowl. If a bowl is almost or completely buried by mobilized fines, the surface would not appear as sharply bounded. A possible example of such is called out in Fig. 3. Hence, one possible reason for the absence of ponds in or around the largest craters on Eros may be that the depth of unconsolidated fines there is too great. The depths of unconsolidated regolith are not uniform over Eros, and in some areas crater infill depths are estimated as many tens of meters (Barnouin-Jha *et al.*, 2001), but in others, it is under ten meters. Psyche and Selene are examples of large craters on Eros, where regolith appears relatively deep (Barnouin-Jha *et al.*, 2001), and where ponds are not found (Robinson *et al.*, 2001). Whether the observed pond distribution on Eros can be explained by the seismic shaking mechanism is not clear, as this mechanism would predict that pond formation depends on the distribution of seismic energy after impacts and on the distribution of regolith depth.

An excessive depth of loose fines may also explain the absence of ponds on Phobos and Deimos, which are deep within the martian gravity well and which therefore re-accrete fines that would have been lost from isolated asteroids of the same size. Nevertheless, it is still a challenge to explain why there are no 1 or 2 km ponds within the 3 km crater or the 6 km crater on Eros. The model suggests a possible explanation, that the equilibration time for shallow gravity waves in such large ponds may be too great. Even a 100 m pond would require tens of globally pond-forming impacts, each of which would create at least a 290 m crater (in the present model)—Eros has only several hundred craters this large. During its sojourn within the Main Belt, Eros may not have experienced enough large impacts to equilibrate ponds much larger than a few hundred meters.

Acknowledgements–This work was supported by NASA under the NEAR project. We thank Peter Thomas, Mark Robinson and Joseph Veverka for helpful comments.

Editorial handling: B. E. Clark

REFERENCES

ADUSHKIN V. AND NEMCHINOV I. (1994) Consequences of impacts of cosmic bodies on the surface of the earth. In *Hazards Due to Comets and Asteroids* (ed. T. Gehrels), pp. 721–778. Univ. Arizona Press, Tucson, Arizona, USA.

ASPHAUG E., KING P., SWIFT M. AND MERRIFIELD M. (2001) Brazil nuts on Eros: Size-sorting of asteroid regolith (abstract). *Lunar Planet. Sci.* **32**, #1708, Lunar and Planetary Institute, Houston, Texas, USA (CD-ROM).

BARNOUIN-JHA O. S., GARVIN J. B., CHENG A. F., ZUBER M., SMITH D., NEUMANN G., MURCHIE S., ROBINSON M. AND VEVERKA J. (2001) Preliminary impact crater dimensions on 433 Eros from the NEAR laser rangefinder and imager (abstract). *Lunar Planet. Sci.* **32**, #1786, Lunar and Planetary Institute, Houston, Texas, USA (CD-ROM).

CARDER D. S. AND CLOUD W. K. (1959) Surface motion from large underground explosions. *J. Geophys. Res.* **64**, 1471–1487.

CHAPMAN C., MERLINE W. J., THOMAS P. C., JOSEPH J., CHENG A. F. AND IZENBERG N. (2002) Impact history of Eros: Craters and boulders. *Icarus* **155**, 104–118.

CHENG A. F., SANTO A., HEERES K., LANDSHOF J., FARQUHAR F., GOLD R. AND LEE S. (1997) Near-Earth asteroid rendezvous: Mission overview. *J. Geophys. Res.* **102**, 23 695–23 708.

CHENG A. F., COLE T., ZUBER M., SMITH D., GUO Y. AND DAVIDSON F. (2000) In-flight calibration of the near-Earth asteroid rendezvous laser rangefinder. *Icarus* **148**, 572–586.

CHENG A. F. *ET AL.* (2001) Laser altimetry of small-scale features on 433 Eros from *NEAR–Shoemaker*. *Science* **292**, 488–491.

CHENG A. F., BARNOUIN-JHA O., PROCKTER L., ZUBER M., NEUMANN G., SMITH D. E., GARVIN J., ROBINSON M., VEVERKA J. AND THOMAS P. (2002) Small-scale topography of Eros from laser altimetry. *Icarus* **155**, 51–74.

COLE T. D., BOIES M. T., EL-DINARY A. S., CHENG A., ZUBER M. T. AND SMITH D. E. (1997) Near-Earth asteroid rendezvous laser altimeter. *Space Sci. Rev.* **82**, 217–524.

GREENBERG R., BOTTKE W., NOLAN M., GEISSLER P., PETIT J-M. AND DURDA D. (1996) Collisional and dynamical history of Ida. *Icarus* **120**, 106–118.

HAWKINS S. E., III *ET AL.* (1997) Multispectral imager on the near-Earth asteroid rendezvous mission. *Space Sci. Rev.* **82**, 30–100.

HOLSAPPLE K. A. (1993) The scaling of impact processes in planetary sciences. *Ann. Revs. Earth Planet. Sci.* **21**, 333–373.

HOUSTON W. N., MORIWAKI Y. AND CHANG C. S. (1973) Downslope movement of lunar soil and rock caused by meteoroid impact. *Proc. Lunar Sci. Conf.* **4th**, 2425–2435.

IVERSON R. M. (1997) The physics of debris flows. *Rev. Geophys.* **35**, 245–296.

JAEGER H. M., NAGEL S. AND BEHRINGER R. (1996) Granular solids, liquids and gases. *Rev. Mod. Phys.* **68**, 1259–1273.

KNIGHT J. B., JAEGER H. AND NAGEL S. (1993) Vibration-induced size separation in granular media: The convection connection. *Phys. Rev. Lett.* **70**, 3728–3731.

LANDAU L. AND LIFSHITZ E. (1959) *Fluid Mechanics*. Pergamon Press, Elmsford, New York, USA. 536 pp.

LEE P. (1996) Dust levitation on asteroids. *Icarus* **124**, 181–194.

MELOSH H. (1989) *Impact Cratering: A Geologic Process*. Oxford Univ. Press, New York, New York, USA. 245 pp.

MICHEL P., FARINELLA P. AND FROESCHLE C. (1998) Dynamics of Eros. *Astron. J.* **16**, 2023–2031.

ROBINSON M. S., THOMAS P. C., VEVERKA J., MURCHIE S. AND CARCICH B. T. (2001) The nature of ponded deposits on Eros. *Nature* **413**, 396–400.

ROSATO A., STRANDBURG K., PRINZ F. AND SWENDSEN R. (1987) Why Brazil nuts are on top: Size segregation of particulate matter by shaking. *Phys. Rev. Lett.* **58**, 1038–1040.

SAVAGE S. B. (1979) Gravity flow of cohesionless granular materials in chutes and channels. *J. Fluid Mech.* **92**, 53–96.

SAVAGE S. B. (1984) The mechanics of rapid granular flows. *Adv. Appl. Mech.* **24**, 289–366.

SCHULTZ P. H. AND GAULT D. E. (1975) Seismically induced modification of lunar surface features. *Proc. Lunar Sci. Conf.* **6th**, 2845–2862.

SHINBROT T. AND MUZZIO F. J. (1998) Reverse buoyancy in shaken granular beds. *Phys. Rev. Lett.* **81**, 4365–4368.

THOMAS P. C., VEVERKA J., ROBINSON M. AND MURCHIE S. (2001) Shoemaker crater as the source of most ejecta blocks on the asteroid 433 Eros. *Nature* **413**, 394–396.

VEVERKA J. *ET AL.* (2000) NEAR at Eros: Imaging and spectral results. *Science* **289**, 2088–2097.

VEVERKA J. *ET AL.* (2001a) Imaging of small-scale features on 433 Eros from NEAR: Evidence for a complex regolith. *Science* **292**, 484–488.

VEVERKA J. *ET AL.* (2001b) The landing of the *NEAR–Shoemaker* spacecraft on asteroid 433 Eros. *Nature* **413**, 390–393.

WILHELMS D. (1984) Moon. In *The Geology of the Terrestrial Planets* (ed. M. Carr), pp. 107–205. NASA SP-**469**, Washington, D.C., USA.

ZUBER M. T. *ET AL.* (2000) The shape of 433 Eros from the NEAR–Shoemaker laser rangefinder. *Science* **289**, 2097–2101.